Efficient harmonic generation in AlGaAs nanoantennas on epsilon-near-zero materials

D. ROCCO,[1,2,*], A. TOGNAZZI[1], L. CARLETTI[3]

[1]*Department of Information Engineering, University of Brescia, Via Branze 38, 25123 Brescia, Italy*
[2]*National Institute of Optics (INO), Via Branze 45, 25123 Brescia, Italy*
[3]*Department of Information Engineering, University of Padova, Via G. Gradenigo, 6/B, Padova, Italy*
**email d.rocco003@unibs.it*

Abstract: Second-harmonic generation from dielectric nanoantennas has been always studied and optimized by properly designing the radiating nanostructures. However, all the strategies have generally failed at limiting the amount of second-harmonic radiation that is lost in the substrate. Here we provide a detailed analysis on the use of epsilon-near-zero substrates to enhance simultaneously SHG conversion and collection efficiency in dielectric nanoantennas. We analyze second-harmonic generation from a cylindrical AlGaAs nanoantenna placed over different substrate materials and we find that when the substrate meets epsilon-near-zero condition at the second harmonic frequency the electromagnetic radiation is efficiently back-scattered and overall efficiency is improved up to three orders of magnitude with respect to other substrate choices. These results let us foresee a novel approach to improve nonlinear processes at the nanoscale and the possibility to realize novel functionalities, such as beam steering and tailored antenna directivities thanks to the tunability of epsilon-near-zero materials.

1. Introduction

High-index dielectric nanoantennas have recently gained interest for many applications such as directional scattering and emission, nonlinear spectroscopy and microscopy [1-4]. In the nonlinear regime, these resonators have also shown the potential to increase conversion efficiencies up to four orders of magnitude with respect to optimized plasmonic nanoantennas when pumped at similar intensities [5-8]. Several approaches have been considered to optimize the nonlinear processes in these structures, but all the strategies have generally failed at limiting the amount of radiation at the harmonic frequencies that is radiated, and therefore lost, in the substrate [9]. It is well known that epsilon-near-zero (ENZ) materials, namely material showing a zero-crossing for the real part of the dielectric permittivity, have peculiar linear properties, such as their ability to realize perfect electromagnetic tunneling and act as good reflectors. For example, it has been demonstrated that an antenna placed on top of an extremely low-permittivity substrate predominantly radiates backward into the air and, therefore, ENZ materials can be effectively used to re-direct antennas electromagnetic radiation [10-13]. Their ability to be good reflectors and, at the same time, provide high electric field values, makes ENZ also good candidates for other purposes, such as energy harvesting, photocatalysis, and nonlinear optical processes [14-22]. With the goal of boosting second harmonic (SH) radiation efficiency, we compare the SH signal radiated from a cylindrical AlGaAs nanoantenna placed over different materials, including an ENZ substrate. We find that the ability to re-direct the electromagnetic radiation is particularly favored when the substrate shows its ENZ condition at the SH frequency. Moreover, the presence of a low-permittivity substrate allows to increase the quality factor of the resonance of the nanoantennas at the fundamental wavelength (FW), improving the scattered SH signal up to three orders of magnitude with respect to a dielectric substrate and up to two orders of magnitude with respect to a metallic one. We finally move to assess the impact of losses in the substrate on the ability to re-direct the radiation at the harmonic frequency and found that the dramatic enhancement in the radiated nonlinear signal comes from the combination of low losses and the ability of the substrate to act as a good reflector. These results suggest that the most efficient approach to improve nonlinear processes

at the nanoscale should be based on the engineering of a whole photonic system rather than on the mere optimization of an ideal, isolated and unloaded nanoresonator.

2. Results and Discussion

We started our investigation by considering an AlGaAs nanocylinder over a semi-infinite substrate [Fig. 1(a)]. As it has been demonstrated by several groups [5, 6, 8, 23], AlGaAs has a strong potential for nonlinear optics since it possesses a high non-resonant quadratic susceptibility ($d_{14} \approx$ 100 pm/V in the near infrared), and a broad spectral window of transparency in the mid-infrared (up to 17 μm), which allows for the generation of intense second-order nonlinear optical effects [24, 25]. We picked an arbitrary height for the nanoantenna, i.e., h = 1 μm, compatible with other AlGaAs structures already realized and tested for the efficient second-harmonic generation [6, 26, 27]. We assumed a x-polarized plane wave excitation at a FW of 4.2 μm and a pump irradiance I_0 = 1.6 GW/cm^2. To model the dispersion of AlGaAs dielectric permittivity we used the analytical model proposed in Ref. [28], that yields $\varepsilon_{\mathrm{AlGaAs,\ FW}}$ = 10.38 at the FW and $\varepsilon_{\mathrm{AlGaAs,SH}}$ =10.54 at the SH. Different substrates were compared to assess their ability to boost the collection of the second harmonic signal. Even though AlGaAs nanoantennas have been usually grown only on few compatible substrates, e.g., AlO_x, novel techniques based on FIB milling will expand the family of viable substrate materials as nanocylinders may be realized from III−V semiconductor nanowires [29]. We studied and compared the optical behavior of the AlGaAs nanoantenna when is placed over an ENZ, a dielectric and a gold substrate. For the ENZ substrate we considered Dy:CdO, which shows its zero-crossing for the real part of the dielectric permittivity around 2 μm [30]. The dielectric permittivity of Dy:CdO is shown in Fig. 1(b). The dispersion of Dy:CdO can be modeled with a single Lorentz oscillator

$$\varepsilon_{ENZ}(\omega) = \varepsilon_{\infty} - \frac{\omega_p^2}{\omega^2 + i\omega\gamma} \tag{1}$$

having the following parameters: ε_{∞} = 5.5, ω_p = 2.3678x10^{15} rad/s and γ = 2.3327x10^{13} rad/s. These parameters yield permittivity values of $\varepsilon_{\mathrm{ENZ,FW}}$ = -22.16 +i 1.43 at the FW and $\varepsilon_{\mathrm{ENZ,SH}}$ = -1.42+i 0.18. Inset of Fig. 1(b) also shows the reflectance for an air/Dy:CdO interface for different incident angles as a function of the excitation wavelength. A careful look at the reflectance map reveals that 100% reflectance is obtained when the incident wavelength is slightly red-shifted with respect to the zero-crossing of the real part of the dielectric permittivity. The best performance from the ENZ substrate is expected when the SH wavelength is tuned in the vicinity of the zero-crossing for the real part of the permittivity, but in a spectral region where 100% reflectance can be observed, i.e. slightly above 2 μm.
For the dielectric substrate we used a dielectric permittivity ε_d = 2.56 both at FW and SH, a value compatible with AlOx [6]. The optical properties of gold are obtained by interpolating the dielectric permittivity values in Ref. [31], which yield a permittivity $\varepsilon_{\mathrm{g,FW}}$ = -700.53 +i 140.98 at the FW and $\varepsilon_{\mathrm{g,SH}}$ = -178.48 +i 24.10 at the SH.

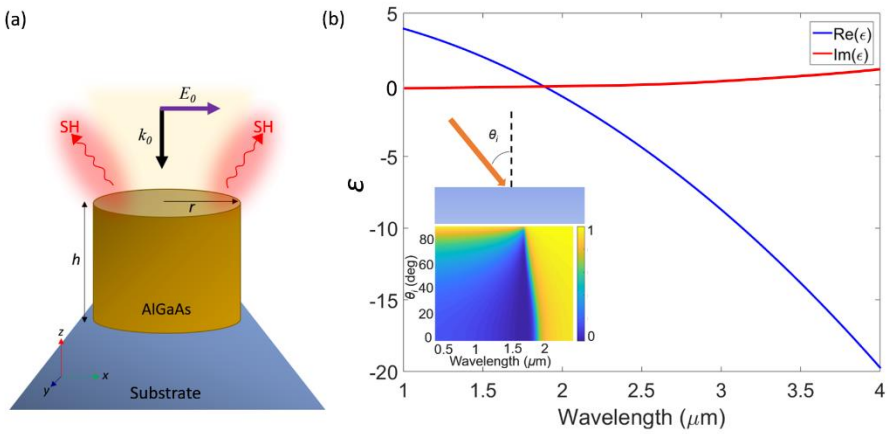

Fig. 1. (a) Sketch of the proposed structure; (b) real and imaginary part of the dielectric permittivity of the Dy:CdO substrate as a function of wavelength. The inset shows the reflectance in the case of air/Dy:CdO interface for different incident angles as a function of the excitation wavelength.

We performed our simulation by means of a commercial software based on the finite element method (Comsol Multiphysics) and evaluated the three different scenarios that have been previously described. First, we investigated the optical scattering of the AlGaAs nanodisk at the FW of 4.2 μm as a function of the nanocylinder radius between 650 nm and 900 nm. As shown in Fig. 2, the maximum scattered power from the 4.2 μm incident beam is obtained for different radii depending on the substrate of choice. For example, by using a Dy:CdO substrate, the scattering power is maximum when the nanoantenna has radius r = 740 nm. The curve for the nanocylinder on AlOx substrate is not reported here since there is no significant scattering peak in the wavelength range of Fig. 2.

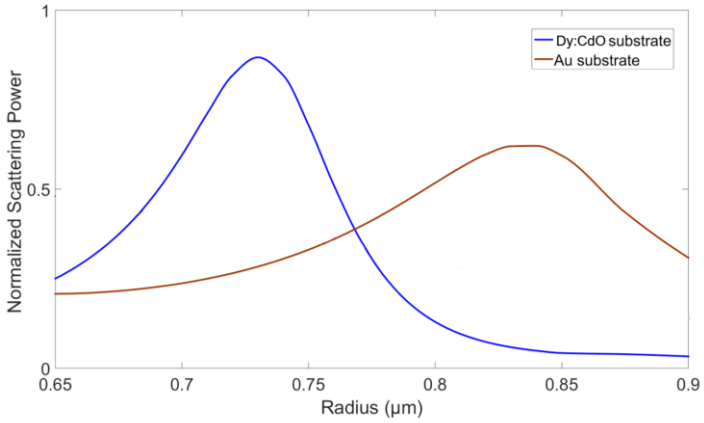

Fig. 2. Scattering power from an incident plane wave at wavelength of 4.2μm as a function of cylinder radius (height of the cylinder is constant, h= 1 μm) for the case of Dy:CdO and gold substrate, I_0=1.6 GW/ cm^2.

Fig. 3 shows the electric field distributions for cylinder radius r = 740 nm on different substrates. More specifically, Fig. 3(a) shows the electric field at the FW when the ENZ material is considered as substrate. The electric field enhancement (FE), defined as the ratio between the electric field norm inside the nanocylinder and the amplitude of the incident field,

achieves a maximum value of ~ 17. The high enhancement of the field at the interface between the substrate and the cylinder can be attributed to the excitation of surface plasmon polaritons of the underlying ENZ material by the dielectric nanoparticle on top [32]. A completely different field localization can be observed with the dielectric substrate: in this case the field circulates inside the disk [see Fig. 3(d)] thanks to the low refractive index of the substrate, triggering sub-wavelength optical confinement in the nanocavity by total internal reflection. Finally, we analyzed the field localization of the nanoantenna placed on a gold substrate: with the metallic substrate the electric field localization is very similar to the ENZ substrate scenario [see Fig. 3(g)]. However, the electric FE for the metallic substrate is significantly lower (~6) than the ENZ substrate. This effect is mostly dependent on the value of the dielectric permittivity: real and imaginary part of ε for gold are respectively one and two orders of magnitude larger than the same quantities in the Dy:CdO substrate at the FW, impacting both field localization and quality factor of the resonance. As the real part of the permittivity of the substrate becomes more negative the electric field generated by the antenna is reduced because the substrate tends to behave like a perfect electric conductor, acting as a short circuit for the scattered electric field and suppressing the resonant response. This phenomenon is similar to what is observed by increasing the imaginary part of the permittivity and can also be understood with the modified mirror image approach: a metallic substrate has the effect of broadening the in-plane magnetic dipole resonance due to interaction with its own in-phase dipole image formed in the substrate and is associated with a decrease in the Q factor of the resonance [33, 34].

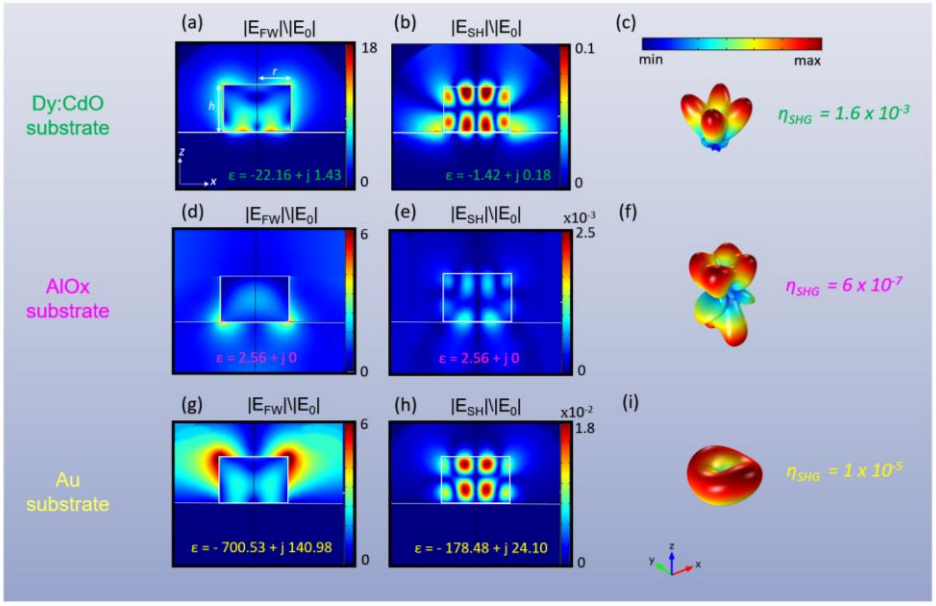

Fig. 3. Electric field enhancement at the FW and SH in the case of nanocylinder with r = 740 nm and h = 1 μm placed over the Dy:CdO [(a) at FW and (b) at SH], the AlOx [(d) at FW and (e) at SH] and the gold substrate [(g) at FW and (h) at SH]; Far-field radiation pattern at the SH for (c) Dy:CdO, (f) AlOx and (i) gold substrates.

We then moved to analyze the nonlinear behavior of these systems. The second-order nonlinear susceptibility tensor of [100]-grown AlGaAs is anisotropic and has only off-diagonal elements $\chi^{(2)}_{i,j,k}$ with $i \neq j \neq k$. The problem at the SH wavelength has been solved by using the calculated fields at the FW to define the second harmonic source as external current density. The i-th component of the external current density J_i is expressed as:

$$J_i = i\omega_{SH}\varepsilon_0\chi^{(2)}E_{FW,j}E_{FW,k}\,, \tag{2}$$

where ε_0 is the vacuum permittivity and $E_{\mathrm{FW,i}}$ ($E_{\mathrm{FW,k}}$) is the i-th (k-th) component of the electric field at the FW. For simplicity we neglected the second order nonlinear contribution coming from the substrates. This assumption does not impact either the conversion efficiencies or the radiation patterns of the SH signal since all materials considered as substrates are centrosymmetric and therefore, they do not possess any second order bulk nonlinearity. Figs. 3(b), (e), and (h) show the electric field distribution at the SH in nanocylinders. For simplicity we considered a radius of 740 nm for all substrate, but we will go back to the optimal radius design later on. Figs. 3(a) and (b) suggest that the use of the an ENZ substrate improves the mode-matching between the mode at FW and SH wavelength. The overlap integral estimation [5] clarifies that the maximum overlap (about 38%) is reached for the ENZ substrate whereas it is about 32% for the gold substrate and 26% for the dielectric substrate. Second harmonic conversion efficiency was then calculated as:

$$\eta_{SHG} = \frac{\int_A S_{SH}\cdot\hat{n}dA}{I_0\pi r^2}, \tag{3}$$

where S_{SH} is the Poynting vector of the SH field, $\hat{n}$ is the unit vector normal to a surface A enclosing the antenna, and I_0 is the incident field intensity. We stress that surface A is placed in the far field of the antenna, therefore the results are independent of the choice of the specific surface. We found a SH conversion efficiency $\eta_{\mathrm{SHG}} = 1.6 \times 10^{-3}$ for the nanoantenna placed over the Dy:CdO substrate. This value well surpasses the SH efficiency achieved with the same AlGaAs nanoantenna placed on either dielectric (AlOx) or gold substrates, respectively of the order of 10^{-7} and 10^{-5}, and also record-high conversion efficiency values of 10^{-5} achieved in experiments [5]. The achieved conversion efficiency of this work is also comparable to theoretical studies of SHG from AlGaAs nanodisks in air based on exploitation of different resonant modes [35]. Figs. 3(c), (f) and (i) also clearly show that, while the Dy:CdO and gold substrate are both able to back-scatter most of the SH signal in the air region, the dielectric substrate can convey only 40% of this energy in the air semi-space.We also stress that, although we compared here all results obtained with a cylinder optimized on the ENZ substrate, no significant improvements can be achieved with the other substrates by changing the cylinder radius, approaching a maximum SH conversion efficiency of $5.5\text{x}10^{-5}$ for a gold substrate (r = 840 nm). The difference in SHG efficiency between the Dy:CdO and gold substrates can be manly attributed to the square of the maximum field enhancement (FE^2) inside the cylinder that is 9 times higher in the case of Dy:CdO substrate with respect to the Au substrate: AlGaAs nanocylinders with radius optimized to yield the best SH conversion efficiencies show FE^2 = 304 for the ENZ substrate (r = 740 nm) and FE^2 = 33.6 for the gold substrate (r = 840 nm). To gain more insight on the increased SH conversion efficiency that we obtained in presence of the ENZ substrate we also calculated the quality factor, Q, of the magnetic-type resonance at the pump frequency supported by the nanoantenna for the ENZ and the metallic substrate (see Fig. 4). Since no significant scattering power peaks can be identified in this spectral range for the AlOx substrate, the Q factor was not evaluated for this specific substrate. We found Q = 28 for the Dy:CdO substrate, which decreases to Q = 17 for the gold substrate for the two optimized radius. We stress that, since the total intensity enhancement inside a nanoparticle is proportional to the product of the so-called coupling efficiency and the resonator efficiency, we find that the structure with the highest Q-factor also achieves the highest conversion efficiency, despite the difficulties to couple the incident energy into a resonator with high Q-factor [36]. In fact, based on a phenomenological picture inspired by temporal coupling mode theory [37], the coupling efficiency of the incident energy to the resonator is proportional to Q^{-1}, while the resonant

intensity enhancement is proportional to Q^2, so that the total intensity enhancement of the field inside the resonator grows linearly with the Q-factor of the resonant mode.

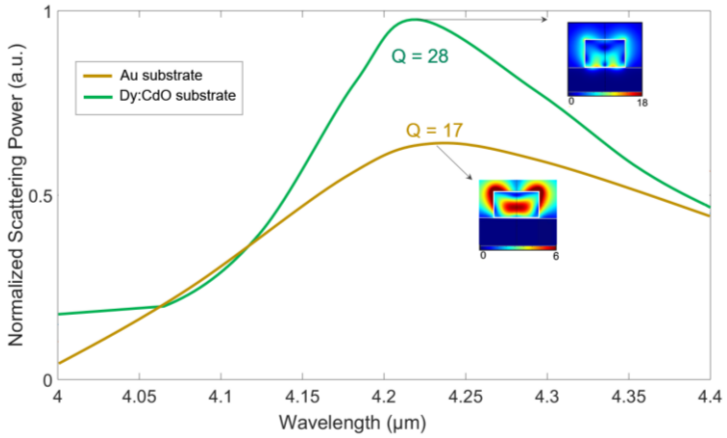

Fig. 4. Green (yellow) line shows the normalized scattering power for an AlGaAs nanoantenna with radius r=740nm (r=840nm) placed over Dy:CdO (gold) substrate. Insets: Near-field distribution of the electric field magnitude for peak scattering power conditions.

Thefore we have demonstrated how the use of an ENZ substrate can significantly improve the conversion efficiency and collection of the second harmonic signal from dielectric nanoantennas. However, both field localization and Q factor analysis do not completely explain the improvement in the SH conversion efficiency when the nanoantenna is placed over the ENZ substrate. ENZ materials are usually characterized by not negligible losses at the zero-crossing of the real part of their permittivity. However, a metallic substrate has an imaginary part of the dielectric permittivity two orders of magnitude higher than the Dy:CdO substrate (see data in Fig. 3). For this reason, assessing the impact of damping on the ability to re-direct the second harmonic signal efficiently is crucial to optimize the system for the nonlinear process. Once again we considered Dy:CdO as the substrate of choice and consider an AlGaAs nanoantenna with the same geometrical parameters described in Section 2.1 (i.e. r = 740 nm, h = 1 μm). The FW is 4.2 μm so that the SH signal is tuned in the vicinity of the zero-crossing for the real part of the permittivity. The substrate is modeled with a single Lorentz oscillator [Eq. (1)] with the following parameters: $\varepsilon_\infty = 5.5$, $\omega_p = 2.3678 \times 10^{15}$ rad/s. To assess the impact of losses we evaluated the second harmonic conversion efficiency by varying the coefficient γ between 10^{11} and 10^{18} rad/s. Fig. 5 summarizes the relation between damping of the substrate and second harmonic efficiency from the nanoantenna, showing that the ability of the substrate to enhance the second harmonic signal is almost constant for values of γ below 10^{13} and decreases dramatically beyond this value [blue line in Fig. 5]. As expected, SH conversion efficiency decreases with the same rate of the electric field enhancement [green line in Fig. 5 shows how FE^2 decreases with increasing damping]. In other words, low losses in the ENZ substrate are crucial to obtain efficient re-direction of the generated harmonic signal that is otherwise absorbed at the second harmonic frequency. Fig. 5 allows us to infer that the inability of a metallic substrate to act as a good substrate for the antenna is mostly because of damping at the harmonic frequency.

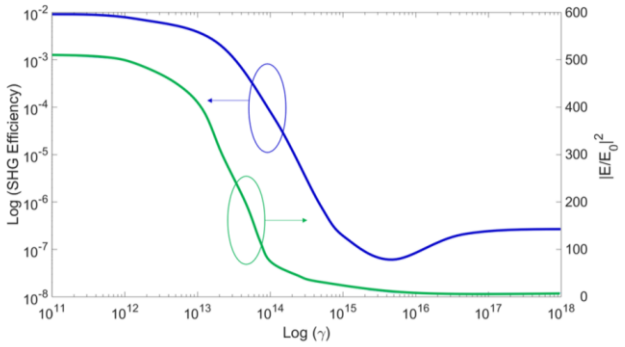

Fig 5. The relation between the losses in the Dy:CdO substrate and the SH efficiency (blue line) generated by the optimized AlGaAs nanodisk (r = 740 nm, h = 1 μm) for a fixed pump intensity I_0=1.6 GW/cm^2. Log-Log scale. The green line represents the relation between the losses in the Dy:CdO substrate and the maximum field enhancement in the cylinder volume.

3. Conclusions

In this work we found that a properly designed AlGaAs nanoantenna placed over an ENZ substrate whose zero-crossing for the real part of the dielectric permittivity occurs in proximity of the SH frequency shows a second harmonic conversion efficiency of the order of 10^{-3} for an input pump of 1.6 GW/cm^2. This value is at least two orders of magnitudes higher compared to the conversion efficiencies obtained with metallic or dielectric substrates and it is similar to ideal free standing AlGaAs nanodisk structures surrounded by air. Second order nonlinear processes from dielectric nanoresonators can be efficiently boosted by exploiting the ability of ENZ materials to act as mirrors, increase the field enhancement in the resonators, while not impacting harmonic generation with significant losses. Thanks to the improved field localization and quality factor of the resonance obtained for the nanoantenna placed over a Dy:CdO substrate we are able to collect almost 100% of the SH generated light. These results demonstrate that ENZ substrate provide the perfect combination of low losses and metal-like behavior to design a novel class of nonlinear photonic metadevices with improved capabilities for on-chip communication, information processing and sensing.

References

1. A. I. Kuznetsov, A. E. Miroshnichenko, M. L. Brongersma, Y. S. Kivshar, and B. Luk'yanchuk, "Optically resonant dielectric nanostructures," Science **354**, aag2472 (2016).
2. D. Smirnova and Y. S. Kivshar, "Multipolar nonlinear nanophotonics," Optica **3**, 1241-1255 (2016).
3. M. Decker and I. Staude, "Resonant dielectric nanostructures: a low-loss platform for functional nanophotonics," Journal of Optics **18**, 103001 (2016).
4. D. Rocco, L. Carletti, A. Locatelli, and C. De Angelis, "Controlling the directivity of all-dielectric nanoantennas excited by integrated quantum emitters," Journal of the Optical Society of America B **34**, 1918-1922 (2017).
5. L. Carletti, A. Locatelli, O. Stepanenko, G. Leo, and C. De Angelis, "Enhanced second-harmonic generation from magnetic resonance in AlGaAs nanoantennas," Optics Express **23**, 26544 (2015).
6. V. F. Gili, L. Carletti, A. Locatelli, D. Rocco, M. Finazzi, L. Ghirardini, I. Favero, C. Gomez, A. Lemaître, M. Celebrano, C. De Angelis, and G. Leo, "Monolithic AlGaAs second-harmonic nanoantennas," Optics Express **24**, 15965 (2016).
7. S. Liu, M. B. Sinclair, S. Saravi, G. A. Keeler, Y. Yang, J. Reno, G. M. Peake, F. Setzpfandt, I. Staude, T. Pertsch, and I. Brener, "Resonantly Enhanced Second-Harmonic Generation Using III–V Semiconductor All-Dielectric Metasurfaces," Nano Letters **16**, 5426-5432 (2016).
8. R. Camacho-Morales, M. Rahmani, S. Kruk, L. Wang, L. Xu, D. A. Smirnova, A. S. Solntsev, A. Miroshnichenko, H. H. Tan, F. Karouta, S. Naureen, K. Vora, L. Carletti, C. De Angelis, C. Jagadish, Y. S. Kivshar, and D. N. Neshev, "Nonlinear Generation of Vector Beams From AlGaAs Nanoantennas," Nano Letters (2016).
9. L. Carletti, G. Marino, L. Ghirardini, V. F. Gili, D. Rocco, I. Favero, A. Locatelli, A. V. Zayats, M. Celebrano, M. Finazzi, G. Leo, C. De Angelis, and D. N. Neshev, "Nonlinear Goniometry by Second-Harmonic Generation in AlGaAs Nanoantennas," ACS Photonics **5**, 4386-4392 (2018).
10. A. Alù, M. G. Silveirinha, A. Salandrino, and N. Engheta, "Epsilon-near-zero metamaterials and electromagnetic sources: Tailoring the radiation phase pattern," Physical Review B **75**, 155410 (2007).

11. M. Silveirinha and N. Engheta, "Tunneling of Electromagnetic Energy through Subwavelength Channels and Bends using ε-Near-Zero Materials," Physical Review Letters **97**, 157403 (2006).
12. S. Enoch, G. Tayeb, P. Sabouroux, N. Guérin, and P. Vincent, "A Metamaterial for Directive Emission," Physical Review Letters **89**, 213902 (2002).
13. G. Lovat, P. Burghignoli, F. Capolino, D. R. Jackson, and D. R. Wilton, "Analysis of directive radiation from a line source in a metamaterial slab with low permittivity," Antennas and Propagation, IEEE Transactions on **54**, 1017-1030 (2006).
14. M. Z. Alam, S. A. Schulz, J. Upham, I. De Leon, and R. W. Boyd, "Large optical nonlinearity of nanoantennas coupled to an epsilon-near-zero material," Nature Photonics **12**, 79-83 (2018).
15. M. A. Vincenti, D. de Ceglia, A. Ciattoni, and M. Scalora, "Singularity-driven second- and third-harmonic generation at ε-near-zero crossing points," Physical Review A **84**, 063826 (2011).
16. A. Ciattoni and E. Spinozzi, "Efficient second-harmonic generation in micrometer-thick slabs with indefinite permittivity," Physical Review A **85**, 043806 (2012).
17. M. Antonietta Vincenti, S. Campione, D. de Ceglia, F. Capolino, and M. Scalora, "Gain-assisted harmonic generation in near-zero permittivity metamaterials made of plasmonic nanoshells," New Journal of Physics **14**, 103016 (2012).
18. A. Ciattoni, C. Rizza, and E. Palange, "Extreme nonlinear electrodynamics in metamaterials with very small linear dielectric permittivity," Physical Review A **81**, 043839 (2010).
19. D. de Ceglia, S. Campione, M. A. Vincenti, F. Capolino, and M. Scalora, "Low-damping epsilon-near-zero slabs: Nonlinear and nonlocal optical properties," Physical Review B **87**, 155140 (2013).
20. C. Rizza, A. Ciattoni, and E. Palange, "Two-peaked and flat-top perfect bright solitons in nonlinear metamaterials with epsilon near zero," Physical Review A **83**, 053805 (2011).
21. M. A. Vincenti, M. Kamandi, D. de Ceglia, C. Guclu, M. Scalora, and F. Capolino, "Second-harmonic generation in longitudinal epsilon-near-zero materials," Physical Review B **96**, 045438 (2017).
22. D. Rocco, M. A. Vincenti, and C. De Angelis, "Boosting Second Harmonic Radiation from AlGaAs Nanoantennas with Epsilon-Near-Zero Materials," Applied Sciences **8**, 2212 (2018).
23. J. Kim, A. Dutta, G. V. Naik, A. J. Giles, F. J. Bezares, C. T. Ellis, J. G. Tischler, A. M. Mahmoud, H. Caglayan, O. J. Glembocki, A. V. Kildishev, J. D. Caldwell, A. Boltasseva, and N. Engheta, "Role of epsilon-near-zero substrates in the optical response of plasmonic antennas," Optica **3**, 339-346 (2016).
24. M. Ohashi, T. Kondo, R. Ito, S. Fukatsu, Y. Shiraki, K. Kumata, and S. S. Kano, "Determination of quadratic nonlinear optical coefficient of AlxGa1−xAs system by the method of reflected second harmonics," Journal of Applied Physics **74**, 596-601 (1993).
25. P. P. Vabishchevich, S. Liu, M. B. Sinclair, G. A. Keeler, G. M. Peake, and I. Brener, "Enhanced Second-Harmonic Generation Using Broken Symmetry III–V Semiconductor Fano Metasurfaces," ACS Photonics **5**, 1685-1690 (2018).
26. D. Rocco, V. F. Gili, L. Ghirardini, L. Carletti, I. Favero, A. Locatelli, G. Marino, D. N. Neshev, M. Celebrano, M. Finazzi, G. Leo, and C. De Angelis, "Tuning the second-harmonic generation in AlGaAs nanodimers via non-radiative state optimization [Invited]," Photon. Res. **6**, B6-B12 (2018).
27. L. Carletti, D. Rocco, A. Locatelli, C. De Angelis, V. F. Gili, M. Ravaro, I. Favero, G. Leo, M. Finazzi, L. Ghirardini, M. Celebrano, G. Marino, and A. V. Zayats, "Controlling second-harmonic generation at the nanoscale with monolithic AlGaAs-on-AlOx antennas," Nanotechnology **28**, 114005 (2017).
28. S. Gehrsitz, F. K. Reinhart, C. Gourgon, N. Herres, A. Vonlanthen, and H. Sigg, "The refractive index of AlxGa1−xAs below the band gap: Accurate determination and empirical modeling," Journal of Applied Physics **87**, 7825-7837 (2000).
29. M. Timofeeva, L. Lang, F. Timpu, C. Renaut, A. Bouravleuv, I. Shtrom, G. Cirlin, and R. Grange, "Anapoles in Free-Standing III–V Nanodisks Enhancing Second-Harmonic Generation," Nano Letters **18**, 3695-3702 (2018).
30. E. Sachet, C. T. Shelton, J. S. Harris, B. E. Gaddy, D. L. Irving, S. Curtarolo, B. F. Donovan, P. E. Hopkins, P. A. Sharma, A. L. Sharma, J. Ihlefeld, S. Franzen, and J.-P. Maria, "Dysprosium-doped cadmium oxide as a gateway material for mid-infrared plasmonics," Nature Materials **14**, 414 (2015).
31. P. B. Johnson and R. W. Christy, "Optical Constants of the Noble Metals," Physical Review B **6**, 4370-4379 (1972).
32. T. Hutter, F. M. Huang, S. R. Elliott, and S. Mahajan, "Near-Field Plasmonics of an Individual Dielectric Nanoparticle above a Metallic Substrate," The Journal of Physical Chemistry C **117**, 7784-7790 (2013).
33. I. Sinev, I. Iorsh, A. Bogdanov, D. Permyakov, F. Komissarenko, I. Mukhin, A. Samusev, V. Valuckas, A. I. Kuznetsov, B. S. Luk'yanchuk, A. E. Miroshnichenko, and Y. S. Kivshar, "Polarization control over electric and magnetic dipole resonances of dielectric nanoparticles on metallic films," Laser & Photonics Reviews **10**, 799-806 (2016).
34. A. E. Miroshnichenko, A. B. Evlyukhin, Y. S. Kivshar, and B. N. Chichkov, "Substrate-Induced Resonant Magnetoelectric Effects for Dielectric Nanoparticles," ACS Photonics **2**, 1423-1428 (2015).
35. L. Carletti, K. Koshelev, C. De Angelis, and Y. Kivshar, "Giant Nonlinear Response at the Nanoscale Driven by Bound States in the Continuum," Physical Review Letters **121**, 033903 (2018).
36. Z. Lin, X. Liang, M. Lončar, S. G. Johnson, and A. W. Rodriguez, "Cavity-enhanced second-harmonic generation via nonlinear-overlap optimization," Optica **3**, 233-238 (2016).
37. H. A. Haus, *Waves and fields in optoelectronics* (Prentice Hall, Incorporated, 1984).